CHALMERS

UNIVERSITY OF TECHNOLOGY

Angle of repose of snow: An experimental study on cohesive properties

(article starts on next page)

Angle of repose of snow: An experimental study on cohesive properties

Tobias Eidevåg [a,b,*], Erik S. Thomson [c], David Kallin [b], Johan Casselgren [d], Anders Rasmuson [a]

[a] Department of Chemistry and Chemical Engineering, Chalmers University of Technology, SE-41296 Gothenburg, Sweden
[b] Contamination and Core CFD, Volvo Car Corporation, SE-40531 Gothenburg, Sweden
[c] Department of Chemistry & Molecular Biology, Atmospheric Science, University of Gothenburg, SE-41296 Gothenburg, Sweden
[d] Division of Fluid and Experimental Mechanics, Luleå University of Technology, SE-97187 Luleå, Sweden

ABSTRACT

The angle of repose is a measure reflecting the internal friction and cohesion properties of a granular material. In this paper, we present an experimental setup and measurements for the angle of repose of snow for seven different snow samples over a large range of temperatures. The results show that the angle of repose is dependent on the fall height, the temperature, and the grain size of the snow. These variables are quantified, and their interdependencies are separately studied. With increased snow temperature, the angle of repose increases, and this can be explained by the presence of a liquid layer on ice that can be thermodynamically stable at temperatures below the melting point of water. With decreasing grain size the angle of repose also increases which is expected since the cohesive energy decreases more slowly than the grain mass. For increasing fall height, the snow grains generally accelerate to larger collisional velocities, yielding a smaller angle of repose. In general, the dimensionless cohesion number was found to largely reflect the dependencies of the variables and is therefore useful for understanding what affects the angle of repose. The results demonstrate that the drag force and collision dynamics of ice grains are important for understanding how snow accumulates on a surface, for example if one desires predicting snow accretion by simulating a dispersed cloud of snow.

1. Introduction

The cohesive properties of snow are important in many engineering and scientific applications. One example is in avalanche research where it has been observed that the dynamic movement of snow covers is sensitive to temperature, especially when temperatures are above $-1°C$ (Heil et al., 2018). Another example is snow accretion on building roofs, which has an influence on the efficiency of solar panels (Borrebæk et al., 2020) and can cause roof failure (Holicky and Sykora, 2009). The presented research is driven by a need in the automotive industry to better understand snow adhesion. Active safety and autonomous systems have increased the need to understand how snow accretes on vehicle sensors (Eidevåg et al., 2019). The phenomenon of snow accretion on sensor surfaces generally involves a dispersed cloud of snow grains that collide, adhere, and accumulate on these surfaces.

The angle of repose α of a granular material (illustrated in Fig. 1) is a micro-mechanical property that reflects the internal friction of the material (Al-Hashemi and Al-Amoudi, 2018). The α of a granular material can generally be regarded as a bulk material property but, as was pointed out by Woodcock and Mason (1988), measured values of α

depend not only on the material but also on the experimental setup used. Snow is a cohesive material where the cohesive properties are contact-time dependent due to sintering. The bond strength between grains in contact increases over time, which causes static approaches to measuring α, such as using a tilting table, to be problematic. Instead, it is advantageous to use a dynamic approach with grains of snow that collide and accumulate to form a heap, as has previously been done when studying snow. To the best of our knowledge, Kuroiwa et al. (1967) were the first to measure the α of snow in this way. In their experiments, they used a hopper to shake snow that then fell through a funnel onto a cylindrical platform. They released snow until a stable heap had been obtained such that α could be measured. They observed that α increased with increasing snow temperature T for $T > -20°C$, and they related their findings to the presence of a liquid-layer on ice that can be thermodynamically stable at T well below the melting temperature of water (Jellinek, 1967; Dash et al., 1995; Dash et al., 2006). They observed a sensitivity to fall height H with larger H yielding smaller α. Willibald et al. (2020) proposed a similar experimental setup where the hopper and funnel were replaced with a sieve. They studied how snow grain shape and T affect the snow's α. They have proposed an empirical model based on their measurements that takes into account

---

Nomenclature

A_p	grain cross-section area (m^2)
Co	Cohesion number
D_B	base diameter (m)
d_A	projected area diameter (m)
d_V	volume-weighted mean projected area diameter (m)
E^*	effective Young's modulus (Pa)
g	gravitational constant (m/s^2)
G^+	activation energy (eV)
H	fall height (m)
h	heap height (m)
k_b	Boltzmann constant (eV/K)
P	length of grain boundary (m)
R^*	effective grain radius (m)

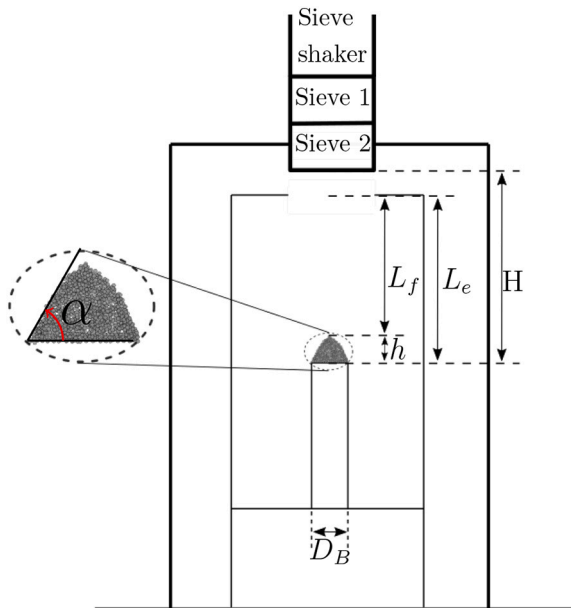|	
s	surface area of sphere (m^2)
S	surface area of grain (m^2)
T	snow temperature (K)
V_i	collisional velocity (m/s)
V_∞	terminal velocity (m/s)
L_e	distance top of inner table to cylinder (m)
L_h	distance top of inner table top to snow heap (m)
W	work of adhesion (J/m^2)
α	angle of repose (°)
δa	uncertainty of quantity a
ϕ	sphericity
$\widehat{\phi}$	circularity
σ	standard deviation
ρ_p	particle density (kg/m^3)

Fig. 1. Experimental setup with important dimensions labeled and the α of snow highlighted in the inset.

shape and T to predict α. In both studies, α was found to be sensitive to T for $T > -15°C$, but few data points were published for this range. The previous studies were also based on relatively large grain sizes and no data for α of snow with an average grain size less than 500 μm has been published, to the best of our knowledge.

In this work, we present and analyze new experimental results for the angle of repose of snow for multiple temperatures greater than $-15°C$ and particles as small as 100 μm. The observations allow us to characterize snow's α as a function of shape, size, T, and H.

The results extend the understanding of the cohesive properties of snow and ice. We show that cohesion is sensitive to T, collisional velocity, and grain properties. The data from this work can be used as validation when simulating snow adhesion and the buildup of snow, for example, using the Discrete Element Method or Smoothed Particle Hydrodynamics. The α for rounded grains at varying T and H reported in this work can also be referred to when validating the cohesive properties of machine made snow.

2. Method and materials

2.1. Experimental setup

Experiments were performed to measure α for different snow samples at different experimental conditions. The experimental setup consisted of a large metal table that held an electric sieve shaker with two sieves (sieve 1 and sieve 2) and a smaller metal table with a solid cylindrical base with diameter D_B (Fig. 1). The purpose of sieving was to shake the snow to separate individual grains. Sieve 1 and 2 had pore sizes 3.15 mm and 2.5 mm, respectively.

An experimental trial was performed by pouring snow into the sieve shaker and shaking the snow sequentially through sieve 1 and sieve 2. The snow grains from sieve 2 fell until they hit the cylinder under the sieve shaker. A growing snow heap formed as more grains accumulated on the cylinder base. Snow was continuously fed into the sieve shaker as long as snow continued to accumulate on the heap. A trial was completed when the height of the cylindrical cone h stopped changing with time, and a measurement usually took a few minutes to complete. To estimate α, h was calculated as

$$h = L_e - (L_f + c), \tag{1}$$

where L_e is the distance between the top of the inner table and the platform without any snow, and L_f is the distance between the top of the inner table and the top of the snow heap. Ideal cones with a sharp vertex at the top of the cone did not always form, and therefore, the length c (as illustrated in Fig. 2) was added as a correction factor.

With the obtained h, α can be calculated as

$$\alpha = arctan\left(\frac{2h}{D_B}\right). \tag{2}$$

The calculated h was estimated to have an uncertainty of $\delta h = 2$ mm, which emerges from measurement uncertainties. The result is a nonlinear and asymmetrical confidence interval for α. However, arctan (x) is a monotonically increasing function and the asymmetry was minor for the values reported in this work. The confidence interval was, therefore, simplified to

$$\alpha \pm \delta\alpha \approx \pm \left(arctan\left(\frac{2(h + \delta h)}{D_B}\right) \right). \tag{3}$$

Alternatively, α could also be measured with image analysis either indirectly using the projected heap area or directly by measuring the angle (Willibald et al., 2020). These methods are sensitive to camera angle, and because the image quality varied in this work, we found that the snow cone height estimate gave the most robust estimate for α.

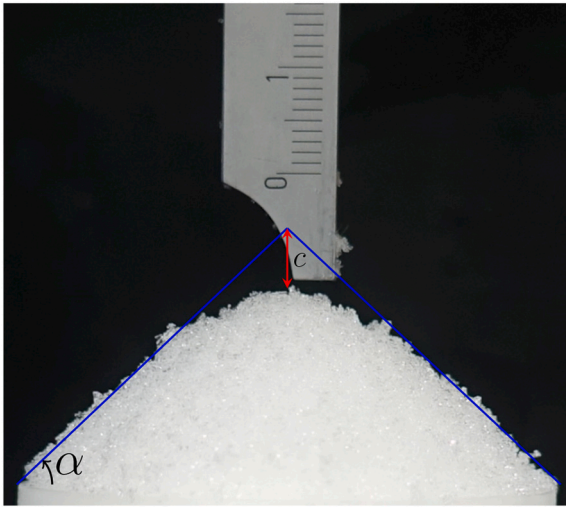Experimental trials were conducted with each snow sample and at

Fig. 2. Illustration of how the height measurements were corrected by adding the length c to the imperfect cone height.

each experimental condition. Average values combining multiple trials were computed, and a conservative error envelope was estimated as,

$$\delta\alpha = max(\delta\alpha_{max}, 2\sigma), \tag{4}$$

where $\delta\alpha_{max}$ is the largest obtained $\delta\alpha$ of the measurements, and σ is the standard deviation of α for the repetitions.

Previous work on the α of snow has shown that α is independent of D_B (Kuroiwa et al., 1967; Willibald et al., 2020). This was also observed in this work when testing diameters from 25 to 100 mm. $D_B = 50$ mm was used in the experiments for the majority of measurements if not stated otherwise, which is the same D_B used by Kuroiwa et al. (1967) and Willibald et al. (2020).

2.2. Snow samples

Snow samples were collected in containers, and total volumes of 20–30 l were collected for each sample. A sample was defined as a collection of snow at a specific time and place. The samples were labeled using the snow shape classes defined in Fierz et al. (2009), and the labels are summarized in Table 1. The samples RG 1, RG 2, RG 3, PP 1, and SH 1 were collected from the ground outdoors, and only the top layer of snow was collected. The sample RG 4 was collected from an underbody panel on an electric vehicle driven 100 km on a snowy road at the same location and during the same period as RG 3. The machine made snow (MM 1 sample) was collected from the ground in a climate wind-tunnel where the snow was created with a snow cannon.

Each sample was characterized by placing microscope slides just below the sieve shaker and collecting particles from each sample onto the slides. The slides were then photographed using a microscope. Fig. 3 shows examples of microscope images for all the snow samples, except

Table 1
Snow characterization and experimental conditions for snow samples. The labels indicate: RG round grains, MM machine made snow, PP precipitation particles and SH surface hoar.

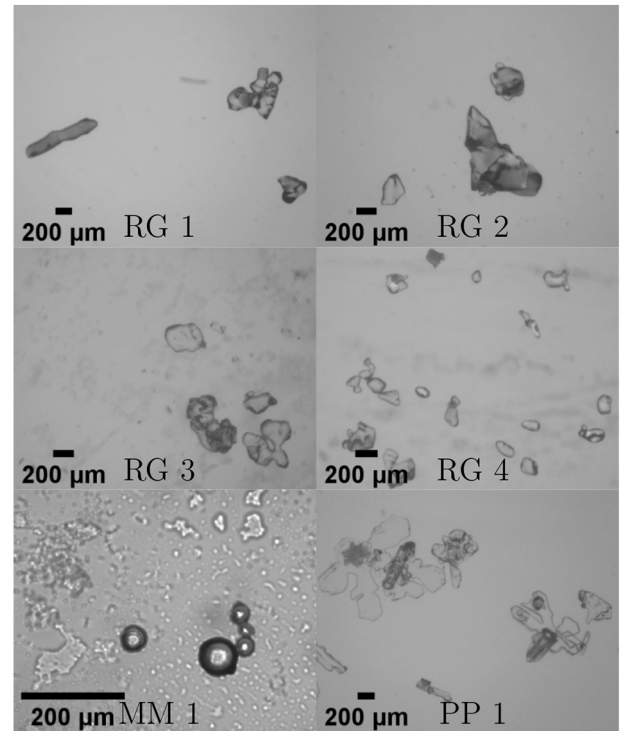| Label	$\widehat{\phi}_m$	d_V [μm]	T [°C]	H [m]
RG 1	0.70	455	−2 to −14	0.07–0.34
RG 2	0.75	775	−1 to −14	0.07–0.25
RG 3	0.72	492	−16 to −27	0.1–0.25
RG 4	0.82	288	−14	0.1–0.25
MM 1	0.95	80	−9 to −13	0.1–0.34
PP 1	N/A	N/A	−12	0.1
SH 1	N/A	N/A	−14	0.1

Fig. 3. Typical microscope images taken of six snow samples.

for the SH 1 sample. The magnification was similar for each sample except for the MM 1 sample, which had a higher magnification due to its small grain sizes. The grain boundaries for each image were extracted with manual segmentation of each boundary using the image analysis program Fiji, and the segments were analyzed to extract grain properties characteristic for each sample. On average, 450 grain boundaries were extracted for each sample with a minimum number of 291 for RG 1. Two properties were extracted for each grain: the projected area diameter, d_A, and the circularity, $\widehat{\phi}$. d_A and $\widehat{\phi}$ are defined as

$$d_A = \sqrt{\frac{4A_p}{\pi}}, \tag{5}$$

and

$$\widehat{\phi} = \frac{4\pi A_p}{P}, \tag{6}$$

where A_p is the grain cross-section area, and P is the length of the grain boundary. $\widehat{\phi}$ was used as an approximation of the sphericity, ϕ, since the microscope slides contained only 2D data, and ϕ is a 3D measure containing the surface area of a grain, defined as

$$\phi = \frac{s}{S}, \tag{7}$$

where s is the surface area of a sphere with the same volume as the grain, and S is the surface area of the grain. However, $\widehat{\phi}$ is often used as an approximation of ϕ, for example for volcanic particles (Bagheri and Bonadonna, 2016).

Experiments measuring α were performed either in cooling chambers or outdoors, depending on the snow sample. The air temperature in the cooling chambers could be controlled. The samples RG 1, RG 2, and PP 1 were measured in a cooling chamber with high precision control of the temperature (± 0.5°C), while RG 3 was measured in a cooling chamber with low precision control of the temperature (± 2°C). Samples RG 4 and SH 3 were measured outdoors. The measurements of the samples RG 1 and RG 2 are the largest datasets of α in this work, where multiple trials

with varying T and H were performed. These two samples were stored in a cooling chamber before measurements to allow the grains to approach an equilibrium shape by means of snow metamorphism. Sample RG 1 was collected after outdoor dry snow metamorphism at a temperature of $-5°C$ and stored for 3 weeks before testing. Sample RG 2 was collected after wet snow metamorphism at a temperature of $0°C$ and was stored at $T = -5°C$ for 4 days before testing.

The grain properties, d_A and $\widehat{\phi}$, for the different snow samples were visualized using a binned histogram showing the normalized frequency of d_A (Fig. 4 and Fig. 5) and a box-plot centered around the median for $\widehat{\phi}$ (Fig. 6). The histograms were normalized such that the sum of the bin heights for each sample is equal to 1. Particle properties, d_A and $\widehat{\phi}$ were not calculated for the PP 1 and SH 1 samples due to the observed shape complexities of these samples. The volume-weighted average projected area diameter d_V, and the median circularity $\widehat{\phi}_m$, for each snow sample are summarized in Table 1. The volume-weighted average was used to weight the volumetric effect a grain has on the overall volume of a snow heap. The MM 1 sample was significantly smaller than any other sample, with $\widehat{\phi} \approx 1$, two properties that are common for machine made snow from snow cannons (Fierz et al., 2009). The d_A range from $100 - 1000$ μm for the rounded grain samples, which implies that the sieve size of 2.15 mm was sufficiently large for the studied snow samples. The RG 4 sample had significantly smaller d_A than any of the other rounded grains, which implies that the collection method used for this sample acted as a grain-size filtering method, where only the smallest grains were lifted by the vehicle and accumulated on the underbody panel. This has been reported before, for example, Abrahamsson et al. (2018) have concluded that the snow that accumulates on the rear of a car is a subset of smaller particles than those present on the ground.

2.3. Experimental data interpretation

The Johnson-Kendall-Roberts (JKR) model has previously been extensively used to predict cohesive forces between ice grains (Eidevåg et al., 2019; Chokshi et al., 1993; Dominik and Tielens, 1997) and we will here use the JKR model to interpret our experimental observations. The model predicts that the cohesive sticking energy E_s for a colliding grain with diameter d, is proportional to $d^{4/3}$ and will thus decrease with decreasing grain size. The gravitational and kinetic energy acting against the cohesion will also be proportional to d but in this case $\propto d^3$ meaning it will decrease faster than the cohesion energy for a decreasing grain size. Therefore, cohesion is predicted to dominate over the grain
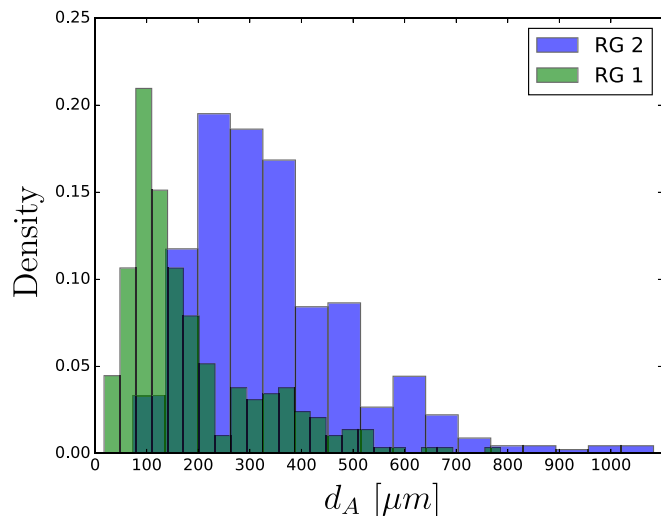

Fig. 4. Normalized particle size distributions determined from image analysis for snow samples RG 1 and RG 2.
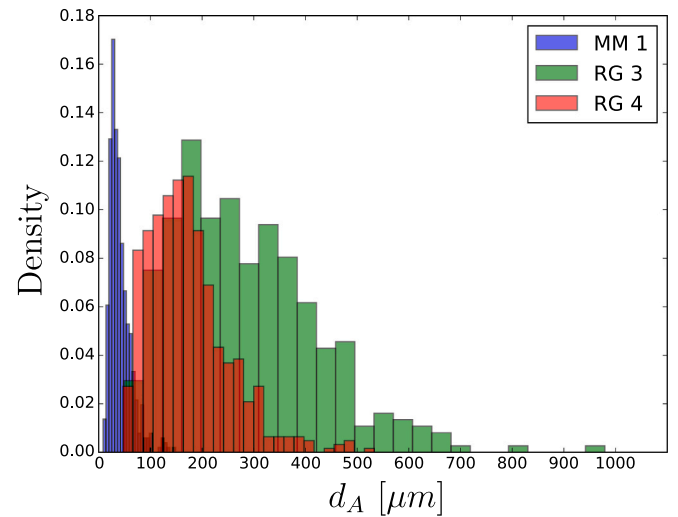

Fig. 5. Normalized particle size distributions determined from image analysis for snow samples MM 1, RG 3, and RG 4.
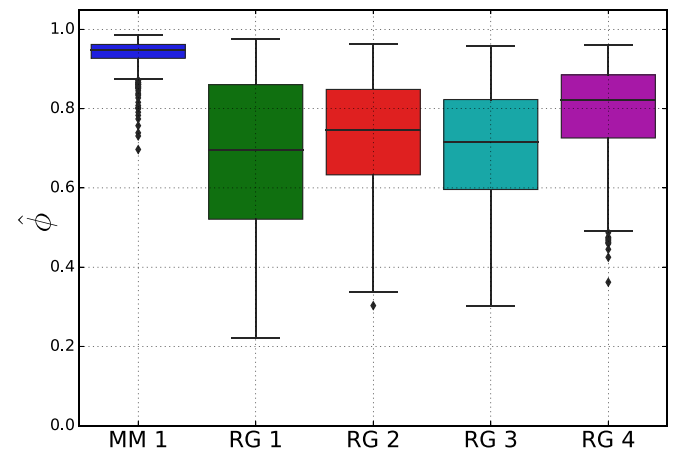

Fig. 6. Snow grain circularity $\widehat{\phi}$ determined from image analysis.

mass for sufficiently small grains and grains will be more cohesive the smaller they are. To better understand these dependencies, we define a dimensionless number Co (the cohesion number) as the ratio between E_s and the kinetic energy at impact, E_i for a single grain impacting a solid wall. Our definition is similar to one proposed by Behjani et al. (2017), except here we use kinetic energy instead of gravitational potential energy. Using the expression for E_s (Eq. 11 in Eidevåg et al. (2019)) and $R^* = 0.5d$, it follows that

$$Co = \frac{E_s}{E_i} \approx \frac{5}{\rho_p V_i^2} \left(\frac{\pi^2 W^5}{d^5 E^{*2}} \right)^{1/3}, \qquad (8)$$

where V_i is the grain collisional velocity, E^* is the effective Young's modulus, W is the work of adhesion and ρ_p is the grain density. For the snow samples in this work, all samples consist of a wide range of grain sizes and to simplify the analysis we will assume that the volume weighted average reflects the overall grain sizes in each sample ($d \approx d_V$).

3. Results and discussion

3.1. General

The α of snow for the different snow samples with $H = 0.1$ m as a function of T are shown in Fig. 7. All measurements presented in this

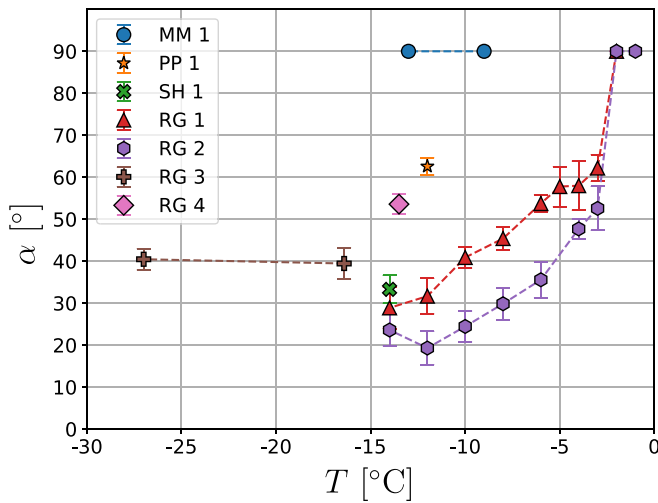**Fig. 7.** The α of snow for the different snow samples as a function of T with H = 0.1 m, where the mean values of repeated trials are plotted with the error bars representing $\delta\alpha$.

Fig. 9. The α of snow for RG 2 as a function of T for different H, where the mean values of repeated trials are plotted with the error bars representing $\delta\alpha$.

figure were done with D_B = 50 mm, except for the RG 4 data, where both 40 mm and 50 mm were used. The figure shows the average values from multiple trials with error bars representing $\delta\alpha$. The experiments generally had good repeatability, which is shown in Appendix A. The magnitude of the α for the different samples varied, for example, the PP 1 sample had an average α = 62° while SH 1 had α = 33°, even though the difference in temperature was minor. Both samples had grains with complex crystalline shapes, but the observed difference implies different cohesion properties. This is in line with previous snow research that has shown that hoar grains have low-cohesive bonds, and they can cause avalanches when present as a layer deep in a snowpack (depth hoar) (Colbeck, 1997; Schweizer and Jamieson, 2001). The results for RG 1 and RG 2 imply that α is strongly dependent on T, which was also observed when H was varied, as shown in Fig. 8 and Fig. 9. At low enough T, lower than -10 or -12 °C, α appears to be constant and independent of T. It was only possible to measure α for the height H = 0.25 m above a certain T (-10°C for RG 1 and -6°C for RG 2) for these two samples. Almost all snow grains bounced away from the base, and no heap of snow formed below this T. This implies a limitation of the experimental setup, where $\alpha \leq 10°$ could not be measured.

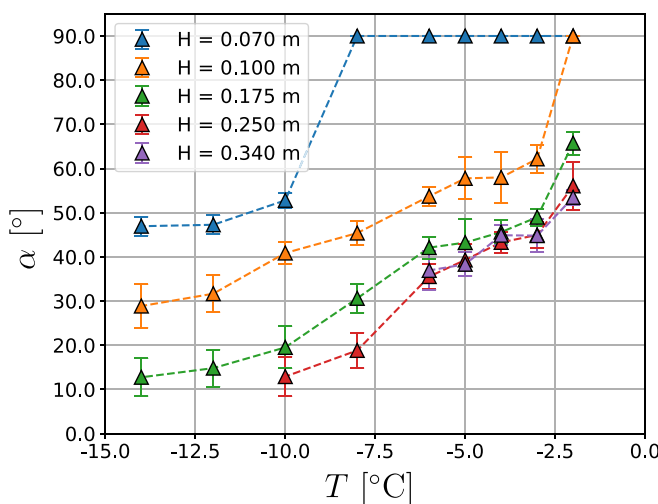In certain trials α = 90° was observed, indicating that a cylindrical

snow heap had formed. The snow heap height observed in these trials increased until the heap touched the sieves. We refer to this phenomenon hereinafter as diverging α, since the α was not well defined. The phenomenon, however, remains interesting because it indicates when cohesive forces dominate over gravity. Fig. 10 shows an example of diverging α for snow sample RG 2 with $T = -1$°C and H = 0.1 m. Diverging α occurred for RG 1 and RG 2 at certain low values of H in combination with T above certain values. We observed diverging α in all measurements of sample MM 1 although the experiments were conducted at a low temperature ($T = -13$°C). This implies that the MM 1 was more cohesive than any of the other snow samples.

Fig. 8. The α of snow for RG 1 as a function of T for different H, where the mean values of repeated trials are plotted with the error bars representing $\delta\alpha$.
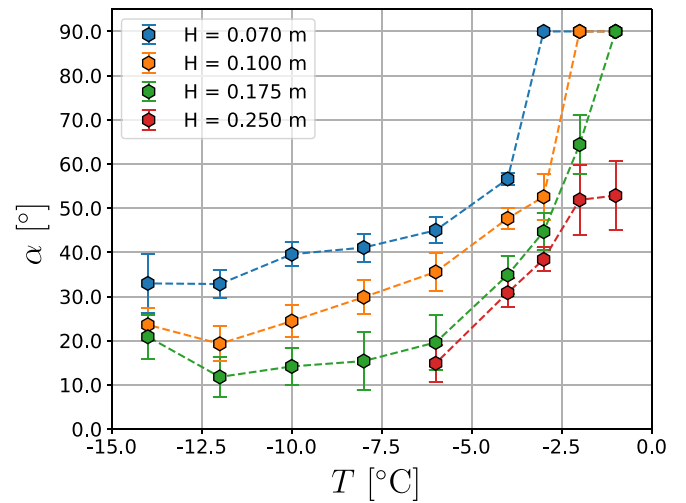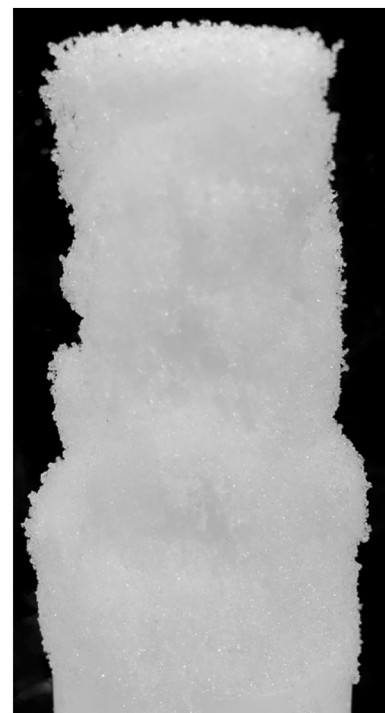

Fig. 10. Experimental trial with diverging α for sample RG 2 with $T = -1$°C and H = 0.1 m.

3.2. Snow temperature

As shown in Figs. 8 and 9 α is sensitive to changes in T and a high T can lead to diverging α as the snow cohesion is strong. Fig. 11 shows α as a function of T for snow samples RG 1, RG 2, and RG 3, as well as measurements from previous studies by Kuroiwa et al. (1967) and Willibald et al. (2020). The data in this figure was measured with $H = 0.1$ m except for the data from Willibald et al. (2020), which used $H = 0.04$ m. The figure shows that α changes for $T \gtrapprox -12°C$. Below this temperature range, α appeared constant and rather independent of T. A comparison with other experimental findings showed that the results reported by Willibald et al. (2020) were rather low given that H was only 0.04 m. This could be due to the larger grains in their samples; they reported grain sizes that ranged from $700 - 1400$ μm. The α reported by Kuroiwa et al. (1967) is similar to the RG 3 sample with values around $40°$.

Jellinek (1967) has studied the cohesion force between ice particles as a function of T. The results showed that cohesion increased with increasing T, and they proposed that the observed T dependency was caused by the existence of a liquid layer on ice that becomes thicker with increasing T. This phenomenon is often referred to as premelting and has been explained by the balance of the intermolecular forces at the surface of ice that causes a liquid layer to form at temperatures below the melting temperature of water (Dash et al., 1995; Dash et al., 2001; Wettlaufer and Worster, 2005; French et al., 2010). Jellinek, used the Arrhenius relation, $\propto \exp(-G^+/k_bT)$, to fit the cohesion force between ice particles as a function of temperature, where G^+ is the activation energy, and k_b is the Boltzmann constant. It is common in ice physics to observe that ice properties have an Arrhenius relation with T. For example, it has been concluded that the creep rate of ice follows an Arrhenius relation but with a sudden increase of activation energy for T approximately above $-15°C$ to $-10°C$ (Weertman, 1983; Cuffey and Paterson, 2006; Goldsby and Kohlstedt, 2001). Goldsby and Kohlstedt (2001) credited this increase to premelting on the surface of ice.

Willibald et al. (2020) have proposed an empirical model for the α of snow, where they use the Arrhenius relation to capture the temperature dependence. Their model can be expressed as,

$$\alpha = A + B\exp(-G^+/k_bT), \tag{9}$$

where A is a sum of the α for cohesionless spheres and a shape correction due to ϕ. In this model, B and G^+ are free parameters. Willibald et al. (2020) obtained $B = 1.5 \cdot 10^{23}$ and $G^+ = 1.2$ eV from curve fitting.

To extract the α dependence on T we performed curve fitting, where the averaged results for samples RG 1 and RG 2 were fitted to Eq. 9 for each individual H. We omitted data points with diverging α, and we have also omitted the data series with $H = 0.07$ m for sample RG 1, because it only contained 3 data points. The resulting least squares fits are shown in Table 2 for the parameters A, B, and G^+ and for the correlation coefficient, R^2. We obtained almost identical activation energies with an average of $G^+ = 1.15$ eV for the eight different series. The best fit of B was, on average, $1.03 \cdot 10^{23}$ with no obvious H dependence. We conclude, therefore, that α has a T dependence that follows an Arrhenius relation independent of H, and that the G^+ we obtained was almost identical to the results reported by Willibald et al. (2020).

3.3. Grain size

The snow samples in this work had a large range of grain sizes. In Section 2.3 we introduced the cohesion number where $Co \propto d_V^{-5/3}$. How α depends on Co is unkown but it is expected that α increases for increasing Co and therefore, samples with smaller d_V should yield smaller α. Previous research has shown that α does depend on particle size and that α increases with decreasing particle size (Cadle, 1965). This can also be seen in our results for the RG 4 sample, which had a significantly higher α than the RG 3 sample, even though the type of grains and grain shape were similar. To assert how α depends on d_V we propose a dependence of the form $\alpha \propto a \cdot d_V^b$, for a constant a and an exponent b.

Fig. 12 shows the α for the snow samples RG 1, RG 2, RG 3, and MM 1 together with a curve fit assuming this proportionality. The effect of temperature difference between the samples was assumed to be negligible since, as shown in Section 3.2, the α dependence was expected to be small for $T \leq -12°C$. The data for the MM 1 sample was excluded from the curve fitting since it is unknown if a diverging α also occurs for $d_V > 80\mu m$ and the fitted line suggests that a diverging α may already occur for $d_V \approx 150$ μm. The obtained best fit for the remaining four data points was $\alpha \propto d_V^{-0.86}$, which suggests that $\alpha \propto Co^{0.86 \cdot 3/5} \approx Co^{0.5}$, however, only a single data point was below 400 μm (RG 4). Thus, we regard the estimated exponent b as uncertain, but the results do show that samples with lower d_V have higher angles of repose.

3.4. Fall height and grain acceleration

Our results show that α is sensitive to H and generally decreases with increasing H. Fig. 13 shows α as a function of H for different samples of rounded grains, at different temperatures. α did not always decrease with an increase in H. Only small changes were observed between $H = 0.17$ m and $H = 0.25$ m, and no change was observed between $H = 0.25$ m and $H = 0.34$ m for RG 1. These observations can be explained by the acceleration of grains when falling. The acceleration of grains does also explain why some of the obtained α for high H is lower than what was previously reported by Willibald et al. (2020) for the α of snow.

When a grain falls in the experiments, it accelerates according to Newton's law of motion, where the acceleration is equal to the difference between the gravitational force and the drag force acting on the grain divided by grain mass. The grain accelerates until either it collides

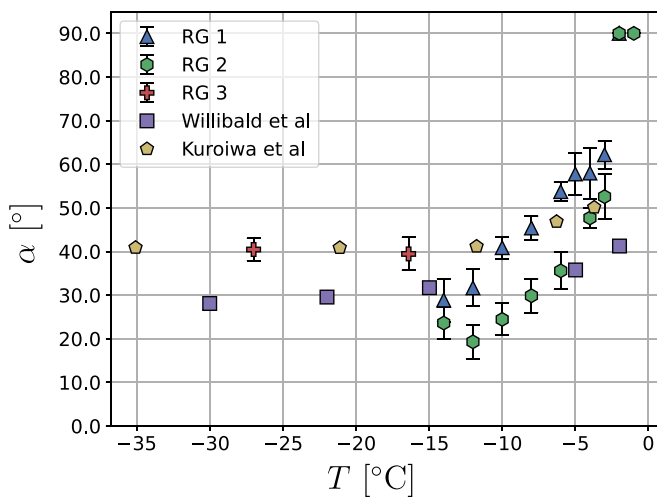**Fig. 11.** The α of snow for samples RG 1, RG 2, and RG 3 as well as previously published results in Willibald et al. (2020) and Kuroiwa et al. (1967) as a function of T.

Table 2
Least squares fits of Eq. 9 for the measured α for the RG 1 and RG 2 samples at varying H.

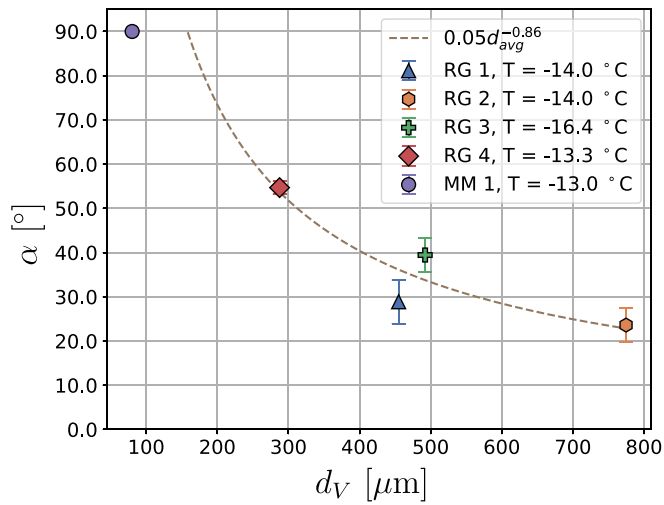| Sample	H	R^2	A	B	G^+ (eV)
RG 1	0.10	0.93	27.84	$0.92 \cdot 10^{23}$	1.15
	0.17	0.95	9.58	$0.99 \cdot 10^{23}$	1.14
	0.25	0.93	4.64	$0.94 \cdot 10^{23}$	1.14
	0.34	0.93	21.86	$0.99 \cdot 10^{23}$	1.16
RG 2	0.07	0.96	28.51	$0.97 \cdot 10^{23}$	1.15
	0.10	0.97	15.32	$1.00 \cdot 10^{23}$	1.15
	0.17	0.85	6.08	$1.20 \cdot 10^{23}$	1.15
	0.25	0.90	1.00	$1.27 \cdot 10^{23}$	1.15

Fig. 12. The α of snow as a function of d_V for the samples RG 1, RG 2, RG 3, RG 4, and MM 1 with $H = 0.1$. The dashed line is the least-squares fitting of the RG samples.
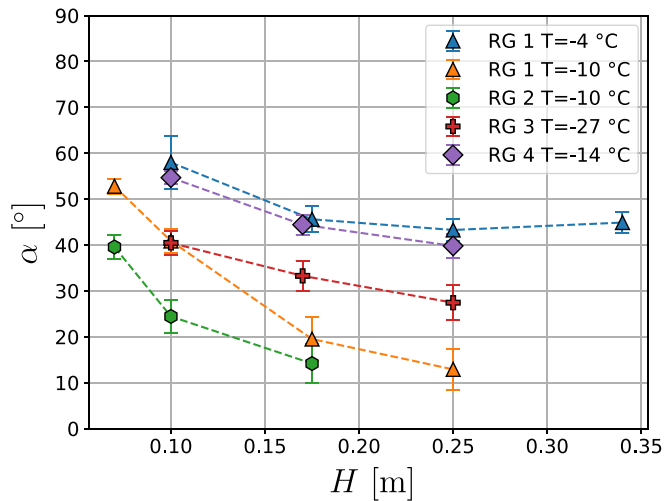

Fig. 14. Predicted V_i of snow grains as a function of H for different grain sizes. Solid lines show spherical grains ($\phi = 1.0$), and dashed lines shows non-spherical grains ($\phi = 0.6$), while the shaded areas show the range between these values of ϕ.

therefore, expect that α will be more sensitive to snow shape for large snow grains. All grains are expected to approach a constant V_∞ with sufficiently high H. Each sample had a distribution of grain size, and therefore, we expected that the V_i would vary between grains in a snow sample. By assuming that the d_V and $\widehat{\phi}$ give an overall representation of the grains in each snow sample the data in Fig. 13 can be replotted as a function of V_i. Fig. 15 shows α as a function of the predicted V_i for different snow samples with rounded grains and at different temperatures. The figure shows that V_i was 1 m/s for most samples and α did not change with minor changes in V_i. For example, the $V_\infty \approx 1.4$ m/s was almost reached at $H = 0.25$ m for the RG 1 sample, which explains why a similar α was obtained for $H = 0.34$ m in Fig. 13.

Previous experiments have shown that collisional damping should increase with increasing V_i for ice grains with sufficiently high V_i (Higa et al., 1998; Eidevåg et al., 2021). A model for collisional melting that explains this phenomenon was proposed by Eidevåg et al. (2021). In the present study, V_i was lower than the theoretical stick velocity for collisional melting and was also lower than the critical velocity for ice particles proposed by Higa et al. (1998). Therefore, we expected the coefficient of restitution for these collisions to be almost constant and

Fig. 13. The α of snow as a function of H for different snow samples with rounded grains and at different T.

with a collisional velocity V_i or reaches its terminal velocity V_∞, which occurs when the two forces are equal. Increasing H, therefore, yields an increase in V_i if $V_i < V_\infty$. The drag force depends on grain size, shape, and the current velocity of the grain. We calculated an estimate of V_i for different grains as a function of H by solving Newton's law of motion using the drag coefficient correlation proposed by Haider and Levenspiel (1989), (cf. their Eq. (11)). The drag coefficient depends on ϕ and the particle Reynolds number Re_p, which is defined as

$$Re_p = \frac{dV_p\rho_f}{\mu},\qquad(10)$$

where V_p is the relative velocity between the particle and the air, and since the air is not moving $V_s = V_i$. In the calculation we used the material properties for air (viscosity μ and density ρ_f) that are valid for $T = -15°C$ (NOAA/NASA/USAF, 1976) and we approximate that $\widehat{\phi} \approx \phi$. In Fig. 14 the calculated V_i for different grain radii as a function of H are shown for ϕ between 0.6 (dashed lines) and 1.0 (solid lines) to reflect the range of values obtained for $\widehat{\phi}$. The difference between non-spherical and spherical grains increased with increasing grain size and H. We,
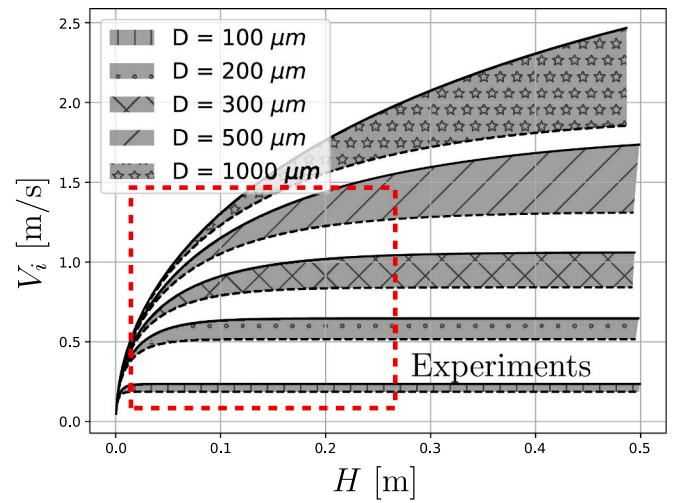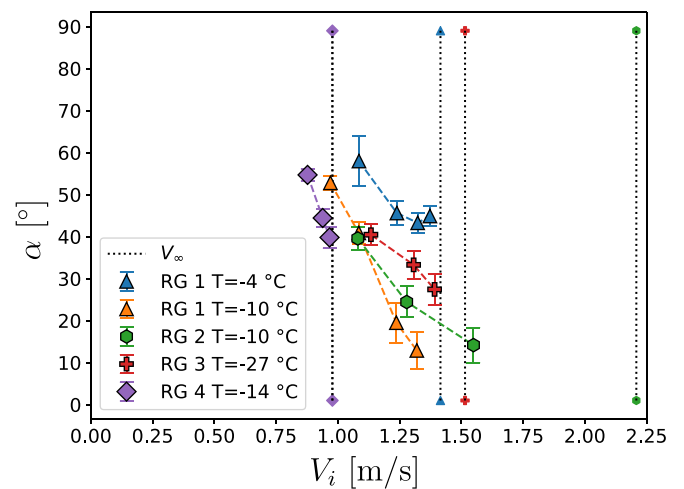

Fig. 15. The α of snow as a function of predicted V_i for different snow samples with rounded grains and different T.

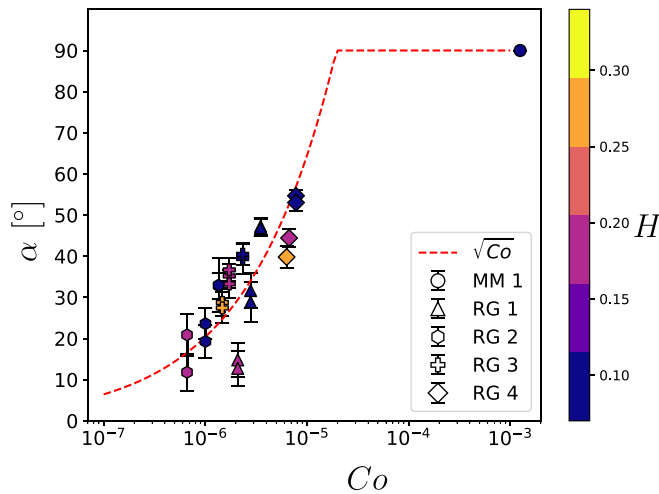**Fig. 16.** The α of snow as a function of Co for different snow samples, with shading indicating H. The mean values of repeated trials are plotted with the error bars representing $\delta\alpha$. Dashed red line showing $\alpha = 20000\sqrt{Co}$. (For interpretation of the references to colour in this figure legend, the reader is referred to the web version of this article.)

only weakly dependent on V_i. This means that the collisions should be in the regime where intermolecular forces dominate sticking and not collisional melting (see regime map in Eidevåg et al. (2021)). During the experiments, the snow grains were observed to rebound from initial collision and bounce multiple times before settling. Consequently, we concluded that more grains fall off the base with increased V_i. This is a likely reason why α is sensitive to H. It also implies that more grains should be able to accumulate with increased D_B. We moreover see that h increased with increasing D_B such that the resulting α was constant.

3.5. The cohesion number

The experimental results shown above imply that $\alpha = \alpha(d_V, \widehat{\phi}, T, H)$. The dimensionless number Co depends on three of these key variables where an explicit relationship to T is missing. It can be argued that $W = W(T)$ due to the existence of a quasi-liquid layer on ice (Eidevåg, 2020), however the exact form is unkown. The experimental results imply that there is only a weak dependence on T for sufficiently low T. α is plotted in Fig. 16 as a function of Co for the experimental measurements with $T \leq -12\,°C$. The material properties W, ρ_p and E^* were taken from what is used in Eidevåg et al. (2019) for ice-ice interactions. The figure also includes the best fit of $\alpha = A\sqrt{Co}$ for $A \approx 20000$ which is based on the dependence $\alpha(Co)$ obtained in Section 3.3. As can be seen in the figure, α generally increases with increasing Co. This is expected given that $Co \propto V_i^{-2} d_V^{-5/3}$, meaning that Co increases with a decrease in d_V or V_i, i.e., the same dependence as observed in the experiments. For most measurements Co ranged from 10^{-6} to 10^{-5}, except for the MM 1 sample, which had the significantly higher value of 10^{-3}. The results, however, show a spread in values and this could be because W might also depend on particle shape, for the proposed Co now $\widehat{\phi}$ will only affect the predicted V_i due to change in drag coefficient. This analysis assumes that d_V gives an overall representation of the grain sizes in each sample, which might be to crude of a simplification.

4. Conclusions

The α of snow is a seemingly simple parameter to study, dispersing a cloud of snow to fall, collide and accumulate on an upright cylinder. The underlying physics for this parameter are, in contrast, highly complex with nonlinear dependencies on multiple variables. We have presented new experimental measurements for the α of snow that extend the knowledge of ice and snow physics, specifically with regards to the cohesion properties of a dispersed cloud of snow. We have shown that α is sensitive to the variables H, T, d_V, and $\widehat{\phi}$, and that these dependencies are nonlinear. We propose that the non-dimensional cohesion number (Co) represents the dependencies for H, d_V, and $\widehat{\phi}$, and we have shown that there is a clear correlation between α and Co for $T \leq -12\,°C$.

The α of snow is sensitive to $T > -12°C$, while it appears rather independent below this range. We have shown that the observed dependence follows an Arrhenius relation, which confirms work by Willibald et al. (2020), and we obtained a similar activation energy (G^+) as in their. These results suggest that $W = W(T)$ however the exact form is unkown.

Our experimental findings for varying H highlight how important this parameter is for the resulting α. For example, the RG 1 sample at $T = -8\,°C$ had an α that varied from $19°$ to $90°$ depending on H. The sensitivity to H was explained by the acceleration of the grains and the resulting V_i. This is a complex relationship that depends on the drag force of the grains and, therefore, depends on both the shape and size of the grains. When modeling snow to predict accretion events, we consequently believe that the drag force and the cohesive properties of snow are important to get right, for example, when using Discrete Element Method or Smoothed Particle Hydrodynamics.

We found that α increases with decreasing d_V for the snow samples studied; machine made snow was the extreme case with diverging α even at $T = -13\,°C$. The α of snow with rounded grains collected outdoors from the ground, ranges from $20°$ to $40°$ for sufficiently low T with $H = 0.1$ m, while increased with increasing T until a diverging α, i. e., $\alpha = 90°$ was reached.

The α of snow can be used as a measure of cohesive properties when creating machine made snow. We have shown that the cohesive properties of a snow sample created with a snow cannon (the MM 1 sample) were significantly different from any naturally collected snow samples with a diverging α for all measurements. A clear difference was also observed between surface hoar crystals (the SH 1 sample) and precipitation particles (the PP 1 sample), where the PP 1 sample had a higher α than the SH 1 sample. These differences imply that measuring the α of snow can be a useful cohesion measure when manufacturing snow, for example, from a snow cannon or with vapor growth in a laboratory, which is a method often used in snow science.

Declaration of Competing Interest

The authors declare that they have no known competing financial interests or personal relationships that could have appeared to influence the work reported in this paper.

Acknowledgments

Appendix A. Repeatability of measurements

The repeatability of the experimental trials was studied to assure the reliability of the measured α. The T studied in this work was close to the melting temperature of water, which makes the snow samples studied sensitive to environmental changes. The morphology of the snow grains was also expected to change over time due to snow metamorphism (Colbeck, 1982). Thus it was important to monitor repeatability to ensure that

morphological changes in snow samples during experimental trials did not affect α. We observed that the experimentally determined α of the same snow sample at the same T was repeatably obtained with little variation between trials. An example is shown in Fig. A.1. The figure shows the experimental measurements of α for sample RG 1 for four different trials at $T = -10°C$. The sample consisted of around 30 l of snow. Ensuring that different snow grains were present in the different measured heaps. However, the α for the different trials were almost exactly the same. For these measurements, the α was estimated to be $41 \pm 3°$. We observed few cases with larger uncertainty, for example, the average value was estimated to be $\alpha = 52 \pm 8°$ for the RG 2 sample, with $T = -2°C$ and $H = 0.25$. However, the changes in α observed for the different T and H in this work were significant compared to the uncertainties.

Measurements of the samples RG 1 and RG 2 were performed over 3 days, and therefore, repeatability was examined during this time by repeating the experiments after 14 h but at the same conditions (with the snow at rest overnight). We observed no statistically significant differences in the α between these trials and, therefore, conclude that the rate of change due to metamorphism was slow and only had a minor influence on the shape and size of the snow grains during the experimental time frame. Repeatability over time was also performed for sample PP 1 to compare freshly collected fallen snow with the same sample aged for 16 h at $-12°C$. We observed a lower α for all measurements of the aged PP 1 sample with an average difference of $4°$. This is expected since fresh snow, with a high specific surface area, has a faster metamorphism rate than granular snow with a low specific surface area (Eppanapelli, 2018).
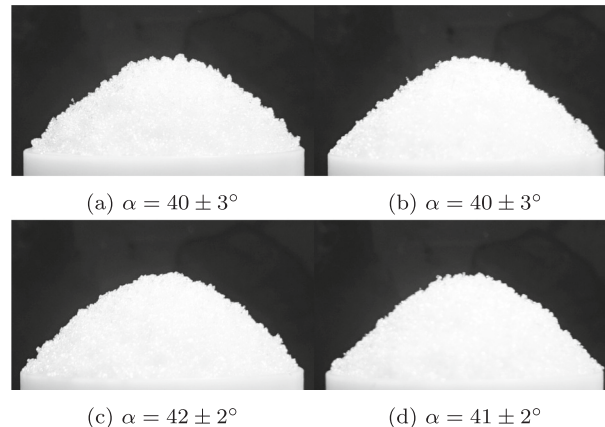

(a) $\alpha = 40 \pm 3°$ (b) $\alpha = 40 \pm 3°$

(c) $\alpha = 42 \pm 2°$ (d) $\alpha = 41 \pm 2°$

Fig. A.1. Four repeated measurements for the α of snow on RG 1 sample at $T = -10°C$ and $H = 0.1$ m.

References

Abrahamsson, P., Eng, M., Rasmuson, A., 2018. An infield study of road snow properties related to snow-car adhesion and snow smoke. Cold Reg. Sci. Technol. 145, 32–39. https://doi.org/10.1016/j.coldregions.2017.09.008.

Al-Hashemi, H.M.B., Al-Amoudi, O.S.B., 2018. A review on the angle of repose of granular materials. Powder Technol. 330, 397–417. https://doi.org/10.1016/j.powtec.2018.02.003.

Bagheri, G., Bonadonna, C., 2016. Aerodynamics of volcanic particles. Volcanic Ash 39–52. https://doi.org/10.1016/b978-0-08-100405-0.00005-7.

Behjani, M.A., Rahmanian, N., Ghani, N. Fardina Abdul, Hassanpour, A., 2017. An investigation on process of seeded granulation in a continuous drum granulator using DEM. Adv. Powder Technol. 28, 2456–2464. https://doi.org/10.1016/j.apt.2017.02.011.

Borrebæk, P.O.A., Jelle, B.P., Zhang, Z., 2020. Avoiding snow and ice accretion on building integrated photovoltaics – challenges, strategies, and opportunities. Sol. Energy Mater. Sol. Cells 206. https://doi.org/10.1016/j.solmat.2019.110306.

Cadle, R.D., 1965. Particle Size - Theory and Industrial Applications. Reinhold Publishing Corporation.

Chokshi, A., Tielens, A.G.G.M., Hollenbach, D., 1993. Dust coagulation. Astrophys. J. 407, 806–819. https://doi.org/10.1086/172562.

Colbeck, S.C., 1982. An overview of seasonal snow metamorphism. Rev. Geophys. Space Phys. 20, 45–61. https://doi.org/10.1029/RG020i001p00045.

Colbeck, S.C., 1997. A review of sintering in seasonal snow. CRREL Rep. 12.

Cuffey, K., Paterson, W.S., 2006. The Physics of Glaciers, 4th editio ed. Academic press. https://doi.org/10.3189/002214311796405906.

Dash, J.G., Haiying, Fu, Wettlaufer, J.S., 1995. The premelting of ice and its environmental consequences. Rep. Prog. Phys. 58, 115–167. https://doi.org/10.1088/0034-4885/58/1/003.

Dash, J.G., Mason, B.L., Wettlaufer, J.S., 2001. Theory of charge and mass transfer in ice-ice collisions. J. Geophys. Res. 106, 395–415. https://doi.org/10.1029/2001JD900109.

Dash, J.G., Rempel, A.W., Wettlaufer, J.S., 2006. The physics of premelted ice and its geophysical consequences. Rev. Mod. Phys. 78, 695–741. https://doi.org/10.1103/RevModPhys.78.695.

Dominik, C., Tielens, A.G.G.M., 1997. The Physics of Dust Coagulation and the Structure of Dust Aggregates in Space. Astrophys. J. 480, 647–673. https://doi.org/10.1086/303996.

Eidevåg, T., 2020. Snow Contamination of Cars: Collisions of Ice Particles with Surfaces. Licentiate thesis. Chalmers University of Technology.

Eidevåg, T., Abrahamsson, P., Eng, M., Rasmuson, A., 2019. Modeling of dry snow adhesion during normal impact with surfaces. Powder Technol. 361, 1081–1092. https://doi.org/10.1016/j.powtec.2019.10.085.

Eidevåg, T., Thomson, E.S., Sollén, S., Casselgren, J., Rasmuson, A., 2021. Collisional damping of spherical ice particles. Powder Technol. 383, 318–327. https://doi.org/10.1016/j.powtec.2021.01.025.

Eppanapelli, L.K., 2018. Experimental Investigation of Snow Metamorphism at near-Surface Layers. Doctoral thesis. Luleå University of Technology.

Fierz, C., Armstrong, R., Durand, Y., Etchevers, P., Greene, E., McClung, D., Nishimura, K., Satyawali, P., Sokratov, S., 2009. The international classification for seasonal snow on the ground. In: IHP-VII Technical Documents in Hydrology, vol. 83, p. 90.

French, R.H., Parsegian, V.A., Podgornik, R., Rajter, R.F., Jagota, A., Luo, J., Asthagiri, D., Chaudhury, M.K., Chiang, Y.M., Granick, S., Kalinin, S., Kardar, M., Kjellander, R., Langreth, D.C., Lewis, J., Lustig, S., Wesolowski, D., Wettlaufer, J.S., Ching, W.Y., Finnis, M., Houlihan, F., Von Lilienfeld, O.A., Van Oss, C.J., Zemb, T., 2010. Long range interactions in nanoscale science. Rev. Mod. Phys. 82, 1887–1944. https://doi.org/10.1103/RevModPhys.82.1887.

Goldsby, D.L., Kohlstedt, D.L., 2001. Superplastic deformation of ice: Experimental observations. J. Geophys. Res. Solid Earth 106, 11017–11030. https://doi.org/10.1029/2000jb900336.

Haider, A., Levenspiel, O., 1989. Drag coefficient and terminal velocity of spherical and nonspherical particles. Powder Technol. 58, 63–70. https://doi.org/10.1016/0032-5910(89)80008-7.

Heil, K., Kaitna, R., Fischer, J.-T., Reiweger, I., 2018. Granulation experiments with snow in a rotating drum, in. Int. Snow Sci. Workshop 21, 94–97.

Higa, M., Arakawa, M., Maeno, N., 1998. Size dependence of restitution coefficients of ice in relation to collision strength. Icarus 133, 310–320. https://doi.org/10.1006/icar.1998.5938.

Holicky, M., Sykora, M., 2009. Failures of roofs under snow load: causes and reliability analysis. In: Forensic Engineering, Proceedings of the Congress, pp. 444–453. https://doi.org/10.1061/41082(362)45.

Jellinek, H.H., 1967. Liquid-like (transition) layer on ice. J. Colloid Interface Sci. 25, 192–205. https://doi.org/10.1016/0021-9797(67)90022-7.

Kuroiwa, D., Mizuno, Y., Takeuchi, M., 1967. Micromeritical porperties of snow. In: International Conference on Low Temperature Science. I. Conference on Physics of Snow and Ice, II. Conference on Cryobiology, pp. 751–772.

NOAA/NASA/USAF, 1976. U.S Standard Atmosphere 1976, Technical Report. U.S. Government Printing, Washington, D.C.

Schweizer, J., Jamieson, J.B., 2001. Snow cover properties for skier triggering of avalanches. Cold Reg. Sci. Technol. 33, 207–221. https://doi.org/10.1016/S0165-232X(01)00039-8.

Weertman, J., 1983. Creep deformation of ice. Annu. Rev. Earth Planet. Sci. 11, 215–240. https://doi.org/10.1146/annurev.ea.11.050183.001243.

Wettlaufer, J., Worster, M.G., 2005. Premelting dynamics. Annu. Rev. Fluid Mech. 38, 427–452. https://doi.org/10.1146/annurev.fluid.37.061903.175758.

Willibald, C., Löwe, H., Theile, T., Dual, J., Schneebeli, M., 2020. Angle of repose experiments with snow: role of grain shape and cohesion. J. Glaciol. 1–9. https://doi.org/10.1017/jog.2020.36.

Woodcock, C.R., Mason, J.S., 1988. Bulk Solids Handling. Springer Netherlands, Dordrecht. https://doi.org/10.1007/978-94-009-2635-6.